Needle and Needleless Electrospinning for Nanofibers

Feng-Lei Zhou, Rong-Hua Gong, Isaac Porat

Textile and Paper, School of Materials, University of Manchester, Manchester M60 1QD, United Kingdom

Received 10 April 2009; accepted 11 August 2009
DOI 10.1002/app.31282
Published online 15 October 2009 in Wiley InterScience (www.interscience.wiley.com).

ABSTRACT: A metallic needle is most often used in conventional electrospinning, where a point-plate electric field with nonuniform distribution is formed in single-needle electrospinning (SNE). Low flow rate in SNE has restricted the application of electrospinning on an industrial scale. Multiple needles have been introduced to enhance the flow rate. However, multiple needles make the electric field distribution much more complex. To resolve this problem, alternative electrospinning setups with more uniform electric field have to be developed. Flat spinnerets have been demonstrated to replace the needle in SNE setups. The operating diagrams for flat spinneret electrospinning (FSE) were determined and differed significantly from those for SNE. Nanofibers produced by FSE were more uniform than those from SNE. These differences were explained by the differences in electric fields simulated using finite element analysis (FEA). © 2009 Wiley Periodicals, Inc. J Appl Polym Sci 115: 2591–2598, 2010

Key words: nanotechnology; fibers; morphology; simulations; electrospinning

INTRODUCTION

In conventional electrospinning setups,[1] a needle is most often used to play a dual role in electrospinning as one electrode for the electric field and also an anchor to suspend the solution droplet. Recently, multineedle electrospinning setups have been developed to produce multicomponent nanofiber webs,[2] but the main objective of multineedle system is to enhance the flow rate of polymer solution and thus the production rate of nanofibers.[3–8] However, some problems occur in multineedle electrospinning, such as configuration complexity and needle clogging. Some efforts on needleless electrospinning have been made to overcome the problems in multineedle processes.[9–14] A detailed comparison between multineedle and needleless electrospinning has been made in a recent review.[15]

In single-needle electrospinning (SNE), an electric field with point-plate configuration forms the Taylor cone, together with surface tension, initiates a jet and then stretches the jet toward a grounded collector. Three other electric field configurations in SNE were also reported.[16] FEA has been widely used to simulate the electric field distribution in SNE with various configurations.[16–21] Previous studies have shown that electric field distribution can influence the cone formation, jet path, as well as the morphology and the size of resultant fibers.[16,20]

A novel spinneret, the "flat spinneret electrospinning (FSE)", has recently been developed in the University of Manchester.[22] This uses a flat plastic spinneret to produce polymeric nanofibers. The advantages of FSE over SNE include more uniform electric field and ease of scaling-up. Here, we report new results where the operating diagrams for SNE and FSE were determined by cycling applied voltage at fixed flow rates. More uniform nanofibers were produced by FSE using the same process variables as for SNE. Possible reasons for the differences in SNE and FSE are discussed based on FEA simulation of electric field.

EXPERIMENTAL

Materials

Polyethylene oxide (PEO, $M_v = 9 \times 10^5$ g/mol, Sigma-Aldrich, Inc., UK) was used as received, whereas distilled water was prepared using double distillation (Fistreem-Cyclon, UK). PEO powder was dissolved in distilled water into solution with 6.0 wt % concentration at the ambient temperature and about 72 h were allowed for the complete dissolution during which the solution was placed on a rotating magnetic mixer (Kika Labortechnik RCT Basic Heater/Stirrer) for gentle mixing.

Electrospinning

Schematic representations of single-needle and single-hole FSE experimental systems with vertical

Correspondence to: F.-L. Zhou (fenglei.zhou@postgrad.manchester.ac.uk).

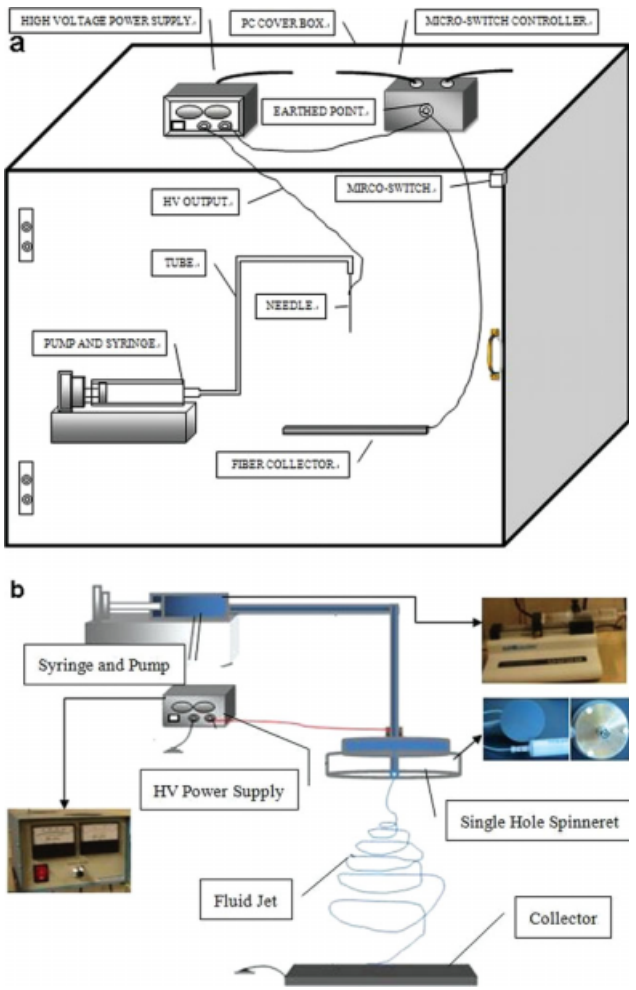

Figure 1 Apparatus diagrams of (a) SNE and (b) single-hole FSE setups (not to scale). [Color figure can be viewed in the online issue, which is available at www.interscience.wiley.com.]

configuration are shown in Figure 1. In SNE, polymer solution in a 20 mL glass syringe was pushed through a flexible Teflon® tube to the metal blunt needle by a syringe pump (Model 100, KD Scientific, UK). The needle was connected to the positive output of the high voltage power supply (ES30P-20W, Gamma High Voltage Research, USA). In the case of FSE, a flat spinneret, comprising a cylindrical plastic solid cap, with a flat end surface, on which one hole was drilled and a metal body, was used to replace the blunt needle in SNE. A grounded aluminum plate was placed below the spinneret to collect nanofibers.

Characterization

Fiber samples for characterization were prepared by cutting a sample of the aluminum foil target and adhering it to a specimen stub with carbon tape and then sputter coating with gold for 2 min (Edwards Sputter Coater S150B) before imaging to minimize charging effect. Electrospun PEO fibers were imaged using a Philips XL-30 SEM (Eindhoven, The Netherlands) with a secondary electron detector at an accelerating voltage of 5 kV. SEM images with the magnifications of 2,500× and 20,000× were used for morphology and size characterization, respectively. From each image, at least 30 different points were randomly selected and their diameters were measured to generate an average value by using NIH ImageJ software (Dr. Wayne Rasband, National Institutes of Health, Bethesda, MD). Fiber diameters were manually measured from three 20,000× images using ImageJ's line-drawing feature that reports line length in pixels. Pixels were converted to standard unit of length measurements using SEM image scale bar.

RESULTS AND DISCUSSION

Operating diagrams

"Operating diagrams" have been used in both electrospraying and electrospinning processes to demonstrate regions of different jet behaviors as a function of applied electric field and flow rate.[23–26] For a given solution, the search for the operating diagrams is of importance in determining the appropriate processing variables of applied voltage, working distance, and flow rate.

Procedurally, for the PEO/water solution, these diagrams were measured by choosing a particular flow rate and then cycling the applied voltage between zero and the maximum voltage of 30 kV. In SNE and FSE, PEO solution first began to accumulate as a droplet suspended on the spinneret exit. It is worth mentioning that the droplet on the needle tip had a larger curvature than that on the surface of flat spinneret. The size of the droplet increased gradually when the applied voltage was increased from 0 kV until a jet comprising straight and spiral segments was ejected from the apex of the droplet at a voltage denoted by V_{start}. When the applied voltage was further increased to the voltage $V_{straight}$, the dual segment of jet started to transform to be a straight jet at a high voltage. On lowering the voltage, the dual-segment jet was resumed and then ceased at a voltage, V_{stop}. For both the SNE and FSE processes, the working distance was set to 17.5 cm. Because dripping was observed at flow rates higher than 4.0 mL/h in SNE, the flow rate was varied from 1.5 to 4.0 mL/h to determine the operating diagrams.

The resultant operating diagrams for SNE and FSE are shown in Figure 2. The three curves represent possible extreme values of jet states in the

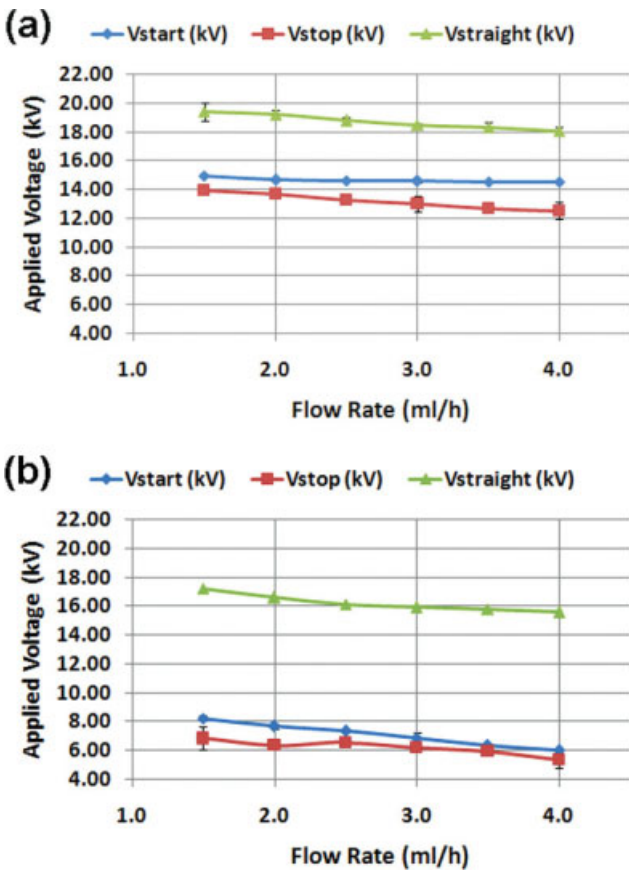

Figure 2 Operating diagrams for (a) FSE and (b) SNE. (▲) $V_{straight}$; (◆) V_{start}; (■) V_{stop}. The region above $V_{straight}$ line: straight jet; The region between V_{start} and $V_{straight}$ lines; straight and bending jet; The region between V_{stop} and V_{start}: straight and bending jet; The region below V_{stop}: no jet. [Color figure can be viewed in the online issue, which is available at www.interscience.wiley.com.]

electrospinning process. The values of $V_{straight}$ decreased with the increasing flow rate in both SNE and FSE processes. This might be explained by the fact that the initial velocity of the jet under higher flow rates was higher, which helped the jet follow a straight path. During the operation of electrospinning in the region above $V_{straight}$ curve, only straight PEO jet was observed, which caused the deposition and coalescence of solution instead of fiber webs. For an electric-driven jet, the bending instability can be suppressed when the tangential external electric field instead of static charge density on the jet dominates for a high conductivity fluid.[27] However, for SNE process in this region, at flow rates less than 1.0 mL/h, only dual-state jet, instead of straight jet was observed with the increasing applied voltage until 19.14 kV when the drop became smaller and the source of the jet moved to the edge of the needle exit. At high electric fields, the average rate at which the solution was forced into the drop by the feed system and the average rate at which the fluid was carried away by the jet were not equal. The region between the $V_{straight}$ and V_{stop} was where a dual-segment jet was obtained. However, the flight path of the dual-state jet formed by the applied voltage between V_{start} and $V_{straight}$, was obviously longer than that of the jet between V_{start} and V_{stop}. Therefore, stable operation of electrospinning in the region between V_{start} and $V_{straight}$ is preferred to produce submicron diameter fibers. Within this region, the length of the straight section of the jet increased with the applied voltage, which was also reported in SNE process with needle-plate configuration electric field.[20,28] The jet completely disappeared and dripping was observed when the applied voltage dropped to the region under the V_{stop} curve. As the flow rate increased in both processes, the values of both V_{start} and V_{stop} mildly decreased and the reason for this can also be understood in terms of jet initial velocity. Moreover, an apparent hysteresis between the onset (V_{start}) and disruption (V_{stop}) of the jet was observed, which coincides with the monotonic results reported in other electrospinning processes of PEO.[23,29] It is also shown in Figure 2, that there are large apparent differences between the values of V_{start} in the SNE and FSE processes while other parameters were maintained constant. This may be partly explained by the fact that PEO solution spread along the flat surface of the spinneret in FSE, which reduced the curvature of the suspended droplet on the spinneret exit and thus higher V_{start} was required to initiate a jet from the apex of the droplet.[30] On the other hand, it has been found that higher voltages have to be applied to achieve a stable electrospinning process under the more uniform electric fields.[20]

FEA simulation

To explain the differences between the SNE and FSE processes, the electric fields were analyzed using Ansoft Maxwell® 2D SV software (ANSYS, USA). Figure 3 shows the electric field and potential distributions calculated by the ANSOFT software based on finite element analysis (FEA). More uniform electric field was produced between the flat spinneret and the collector in FSE than that in SNE, as shown in Figure 3(a,b). The uniformity was further confirmed by Figure 3(c), which indicates the electric field strength along the working distance in the SNE and FSE processes. There was a sharp decrease in electric field strength in SNE but a gradual decrease in FSE. It was reported that the electric field with more uniform distribution can result in the fibers with smaller diameters.[20] Especially, in the SNE process, the local electric field strength in the vicinity of the spinneret [<16.5 mm below the

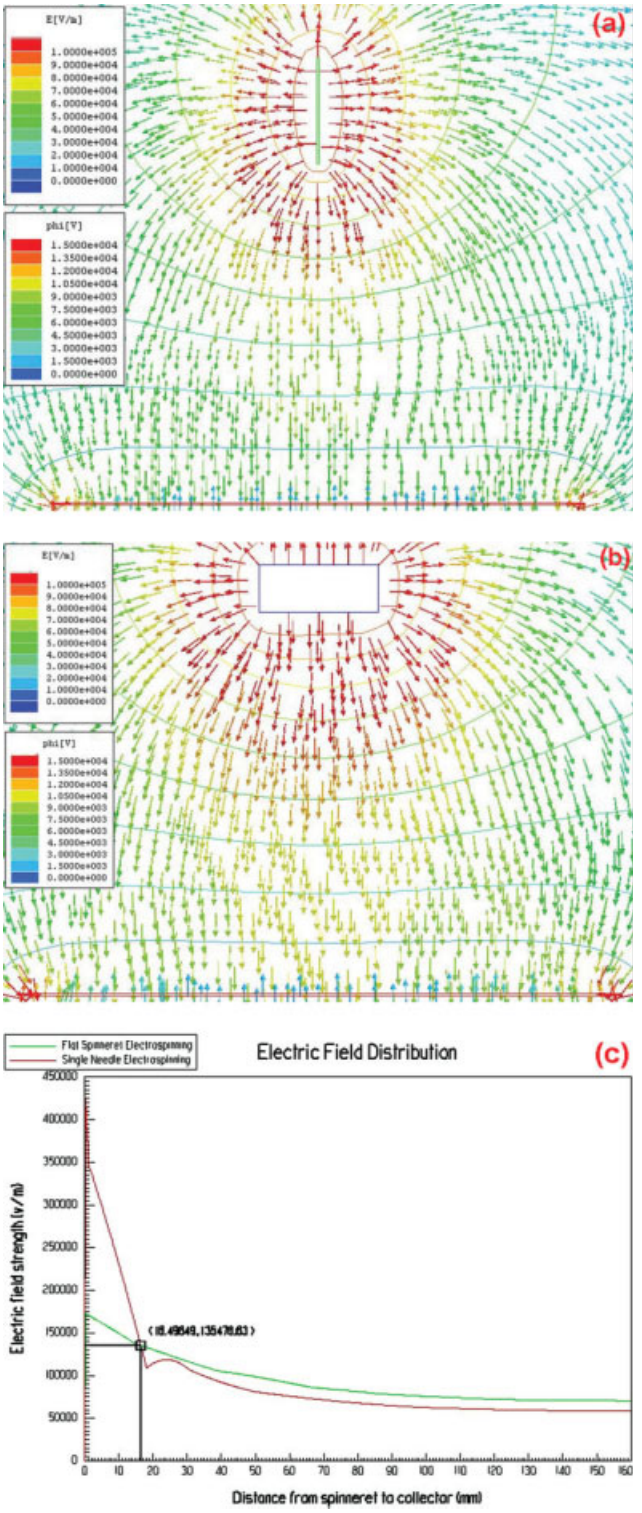

Figure 3 FEA simulations of (a) SNE and (b) FSE process; (c) electric field strength distribution along the working distance from the spinneret to the collector. [Color figure can be viewed in the online issue, which is available at www.interscience.wiley.com.]

spinneret, as shown by the marker in Figure 3(c)] was significantly higher than in the FSE process under the same applied voltage and working distance, which may further account for the lower V_{start} in SNE.

Comparison of nanofibers from FSE and SNE

A systematic comparison was made between FSE and SNE nanofibers produced under the same experimental conditions. As shown in Figure 2, the overlap region of two operating diagrams was quite narrow, where stable processes of FSE and SNE were achieved. Various process variables after optimization are listed in Table I. Figures 4 and 5 show SEM images of PEO nanofibers produced by SNE and FSE. In most cases, the distribution of PEO fibers obtained from SNE was broader than that from FSE, which may be caused by the less uniform electric field distribution in FSE.

Effect of applied voltage

All nanofibers by FES at three different applied voltages had smooth and uniform morphology without bead defects present, as shown in Figure 4(a–c). Less smooth morphology was observed in the case of SNE nanofibers, especially at 16.14 kV, where there were a few beaded fibers with large sizes [Fig. 5(c)]. Previous studies have shown that applied voltage in SNE is strongly correlated with the formation of bead defects in electrospun fibers because of its effect on the shape of the originating droplet suspended on the needle tip. For instance, Deitzel et al.[31] observed that the bead defect density on PEO nanofibers increased with increasing applied voltage. PEO fibers were still wet when they reached the collector under at higher voltages in the SNE process, as evidenced by the present fiber junctions and merging in the nonwoven web [Fig. 5(b,c)]. This was likely to be caused by the fact the values of applied voltage approached the $V_{straight}$ at 2.0 mL/h, as shown in Figure 2(b).

There was no apparent effect of increasing applied voltage on the average fiber diameter in FSE, but a monotonically increasing relationship in SNE. This may reflect that FSE was not so sensitive to small

TABLE I
Experimental Parameters in SNE and FSE Processes

Polymer Solution	Applied voltage (kV)	Working distance (cm)	Flow rate (ml/h)
6.0 wt. % PEO	15.72	17.5	2.0
	15.90	17.5	2.0
	16.14	17.5	2.0
	15.90	17.0	2.0
	15.90	18.0	2.0
	15.90	17.5	1.5
	15.90	17.5	2.5

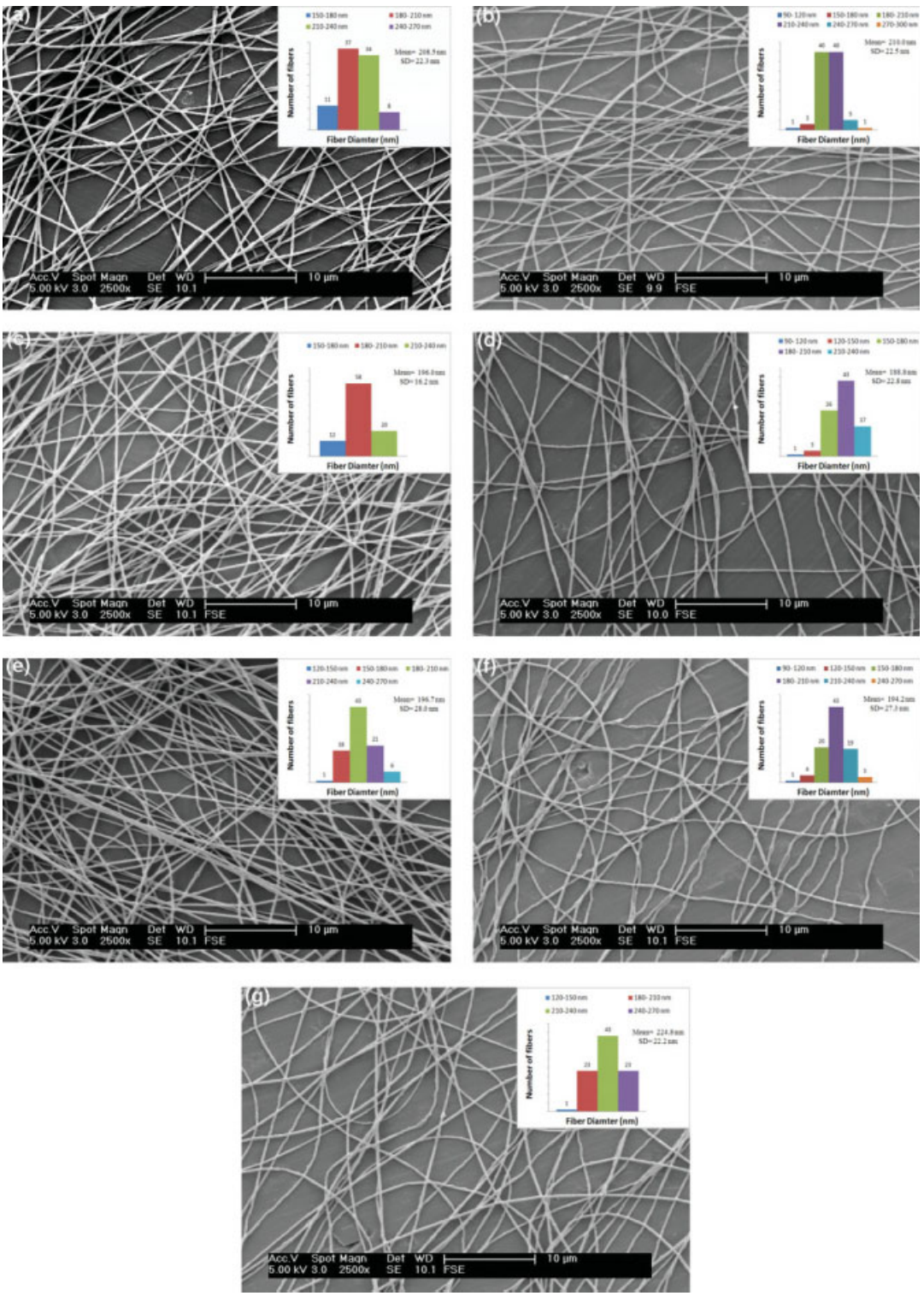

Figure 4 SEM micrographs and size distributions of PEO nanofibers produced by FSE at various applied voltages: (a) 15.72 kV, (b) 15.90 kV, and (c) 16.14 kV; working distances: (d) 17.0 cm and (e) 18.0 cm; flow rates (f) 1.5 mL/h and (g) 2.5 mL/h. [Color figure can be viewed in the online issue, which is available at www.interscience.wiley.com.]

changes in applied voltage as SNE due to its more uniform electric field distribution. The vast majority of PEO fibers from both FSE and SNE had a average diameter of about 200 nm, except those produced at 16.14 kV in SNE.

Effect of working distance

Working distance did not exhibit significant effect on morphology of both FSE and SNE nanofibers. For example, smooth PEO fibers with average diameters

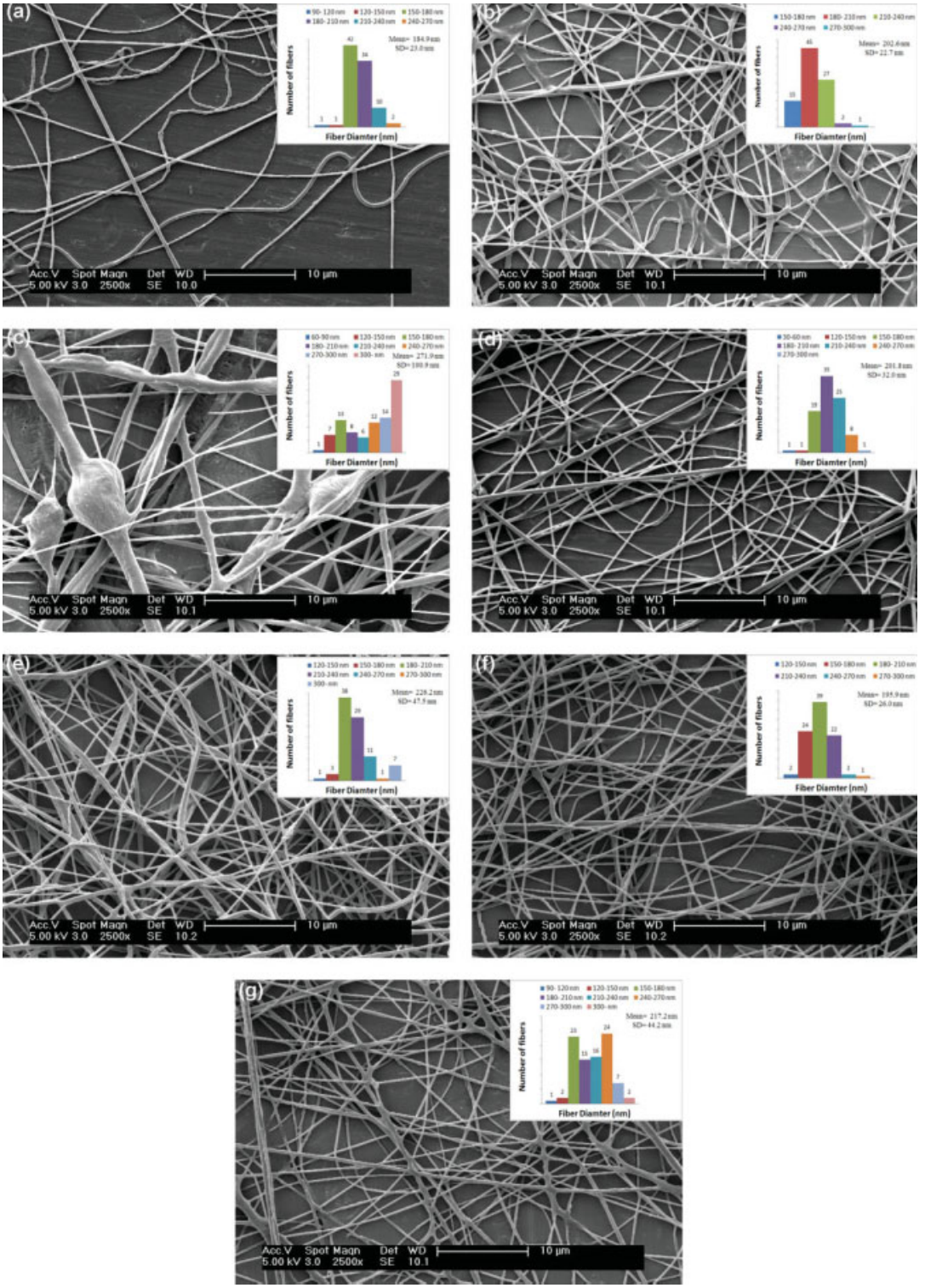

Figure 5 SEM micrographs and size distributions of PEO nanofibers produced by SNE at various applied voltages: (a) 15.72 kV, (b) 15.90 kV, and (c) 16.14 kV; working distances: (d) 17.0 cm and (e) 18.0 cm; flow rates (f) 1.5 mL/h and (g) 2.5 mL/h. [Color figure can be viewed in the online issue, which is available at www.interscience.wiley.com.]

ranging from 180 to 210 nm were fabricated by FSE using three different working distances [Fig. 4(b,d,e)]. SNE nanofibers also showed bead-free structure, though these fibers deposited on the collector in a wet state. The average fiber diameter was found to initially increase with working distance,

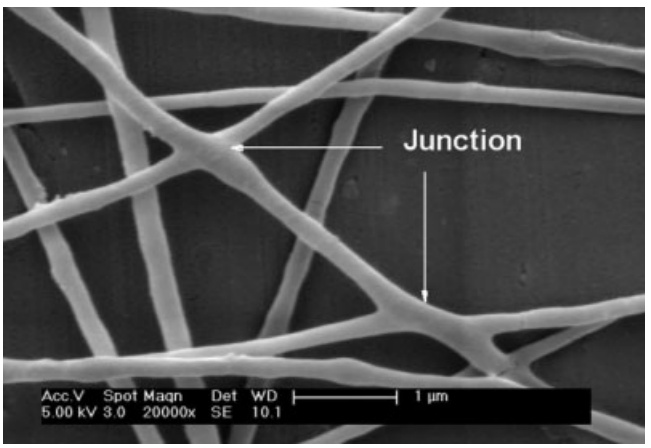

Figure 6 SEM micrograph with 20,000 magnification of PEO nanofibers produced by SNE at 15.72 kV, 17.5 cm, and 2.5 mL/h showing fiber junctions.

and then decrease in FSE. The opposing effects of working distance on average fiber diameter have been reported.[32] Increasing fiber diameter due to higher working distance can be easily explained, since electrostatic forces on the jet became weaker. On the other hand, higher working distance may enhance the jet flight distance and solvent evaporation, which both favor the formation of thinner fibers. In SNE, however, a monotonic increase in average nanofiber average diameter with increasing working distance. A significant fraction of PEO fibers with large diameters were observed at the working distance of 18.0 cm [Fig. 5(e)], which may result from the reduced stretching of the jet under the longer working distance.

Effect of flow rate

Among the various process parameters in SNE, flow rate had the least important effect on the morphological changes of nanofibers.[33,34] In this study, the morphology of PEO nanofibers also slightly changed with the increase in flow rate from 1.5 to 2.5 mL/h. For example, merging was observed at the points of contact among the SNE fibers produced at 2.5 mL/h, showing higher flow rate worsened the wet state [Fig. 5(g)]. However, the smooth bead-free nanofibers were produced by both FSE [Fig. 4(b,f,g)] and SNE [Fig. 5(b,f,g)]. The average diameters of electrospun PEO fibers in these two cases were found to increase monotonically with the increasing flow rate. The overall distribution of fiber diameters created by SNE became broader. A bimodal distribution of fiber diameters was observed and centered at around 165 and 255 nm, respectively [Fig. 5(g)]. A possible explanation for the existence of a bimodal distribution was the formation of lots of junctions due to fiber merging resulting in fluid transfer among the nanofibers, as shown in Figure 6.

CONCLUSIONS

We investigated the operating diagrams and the effects of process variables on the resultant nanofibers in the SNE and FSE processes. The differences between those processes were observed and also explained using FEA simulation of electric field. The electric field was found to be more uniform in FSE than in FSE and this could help scaling up of the spinneret in FSE by using multiple holes to increase the throughput of electrospun nanofibers. The uniformity of the electric field in FSE also led to more uniform nanofibers being produced.

References

1. Teo, W. E.; Ramakrishna, S. Nanotechnology 2006, 14, R89.
2. Ding, B.; Jimura, E.; Sato, T.; Fujita, S.; Shiratori, S. Polymer 2004, 45, 1895.
3. Bowman, J.; Taylor, M.; Sharma, V.; Lynch, A.; Chadha, S. Mat Res Soc Symp Proc 2002, 752, AA1.5.1.
4. Theron, S. A.; Yarin, A. L.; Zussman, E.; Kroll, E. Polymer 2005, 46, 2889.
5. Tomaszewksi, W.; Szadkowski, M. Fibers Textiles East Eur 2005, 13, 22.
6. Kim, G. H.; Cho, Y. S.; Kim, W. D. Eur Polym J 2006, 42, 2031.
7. Yang, Y.; Jia, Z.; Li, Q.; Hou, L.; Gao, H.; Wang, L.; Guan, Z. The 8th International Conference On Properties and Applications of Dielectric Materials, 2006; Bali, Indonesia, p 940.
8. Yang, Y.; Jia, Z.; Li, Q.; Hou, L.; Guan, Z. J Phys Conf Ser 2008, 142, 012027.
9. Yarin, A. L.; Zussman, E. Polymer 2004, 45, 2977.
10. Dosunmu, O. O.; Chase, G. G.; Kataphinan, W.; Reneker, D. H. Nanotechnology 2006, 17, 1123.
11. Huang, X.; Wu, D.; Zhu, Y.; Sun, D. IEEE-NANO, 2007; Hong Kong, p 823.
12. Srivastava, Y.; Thorsen, M. M. T. J Appl Polym Sci 2007, 106, 3171.
13. Lukas, D.; Sarkar, A.; Pokorny, P. J Appl Phys 2008, 103, 0843091.
14. Varabhas, J. S.; Chase, G. G.; Reneker, D. H. Polymer 2008, 49, 4226.
15. Zhou, F. L.; Gong, R. H.; Porat, I. Polym Int 2009, 58, 331.
16. Kong, C.; Lee, T.; Lee, S.; Kim, C. J Mater Sci 2007, 42, 8106.
17. Deitzel, J. M.; Kleinmeyer, J. D.; Hirvonen, J. K.; Beck Tan, N. C. Polymer 2001, 42, 8163.
18. Yang, Y.; Jia, Z.; Guan, Z. IEEE International Conference on Dielectric Liquids, 2005; Coimbra, Portugal, p 457.
19. Pan, C.; Han, Y. H.; Dong, L.; Wang, J.; Gu, Z. Z. J Macromol Sci Part B Phys 2008, 47, 735.
20. Yang, Y.; Jia, Z.; Liu, J.; Li, Q.; Hou, L.; Wang, L.; Guan, Z. J Appl Phys 2008, 103, 104307.
21. Carnell, L. S.; Siochi, E. J.; Wincheski, R. A.; Holloway, N. M.; Clark, R. L. Scr Mater 2009, 60, 359.
22. Zhou, F. L.; Gong, R. H.; Porat, I. Polym Eng Sci, to appear.

23. Shin, Y. M.; Hohman, M. M.; Brenner, M. P.; Rutledge, G. C. Polymer 2001, 42, 09955.
24. Cloupeau, M.; Prunet-Foch, B. J Electrostat 1989, 22, 135.
25. Hohman, M. M.; Shin, M.; Rutledge, G. C.; Brenner, M. P. Phys Fluids 2001, 13, 2221.
26. Wang, C.; Hsu, C. H.; Hwang, I. H. Polymer 2008, 49, 4188.
27. Taylor, G. Proc R Soc 1969, 313, 453.
28. Kowalewski, T. A.; Barral, S. Bull Pol Acad Sci Tech Sci 2005, 53, 385.
29. Doshi, J.; Reneker, D. H. J Electrostat 1995, 35, 51.
30. Byun, D.; Lee, Y.; Quang Tran, S. B.; Nugyen, V. D.; Kim, S.; Park, B.; Lee, S.; Inamdar, N; Bau, H. H. Appl Phys Lett 2008, 92, 093507/1.
31. Deitzel, J. M.; Kosik, W.; Mcknight, S. H.; Tan, N. C.; Crette, S. Polymer 2001, 43, 1025.
32. Heikkiland, P.; Harlin, A. Eur Polym J 2008, 44, 306.
33. Kattamuriand, N.; Sung, C. Mater Res Soc Symp Proc 2003, 788, 141.
34. Zhang, C.; Yuan, X.; Wu, L.; Han, Y.; Sheng, J. Eur Polym J 2005, 41, 423.